Electronic Supplementary Material (ESI) for CrystEngComm.
This journal is © The Royal Society of Chemistry 2019

Supplementary Material (ESI) for CrystEngComm 2019

New two-dimensional Cd(II) coordination networks bearing benzimidazolyl-based linkers as bifunctional chemosensors for detection of acetylacetone and Fe^{3+}

Yong-Sheng Shi, Yue-Hua Li, Guang-Hua Cui, Gui-Ying Dong*

College of Chemical Engineering, Hebei Key Laboratory for Environment Photocatalytic and Electrocatalytic Materials, North China University of Science and Technology, Tangshan Hebei 063009, P. R. China

*Corresponding author: Gui-Ying Dong

Fax: +86-0315-8805462. Tel: +86-0315-8805460

E-mail: tsdgying@126.com.

Table Titles:

Table S1. Crystal and refinement data for complexes **1** and **2**

Table S2. Selected bond lengths [Å] and angles [°] for complexes **1** and **2**

Table S3. Simulated in different environments at room temperature

Table S4. Comparison of the sensitivities of **1** and **2** for acac with related CPs

Table S5. Comparison of the sensitivities of **1** and **2** with previously reported CPs to Fe^{3+} ions

Table S1 Crystal data and structure refinements for the **1** and **2**

CP	**1**	**2**
Chemical formula	$C_{33.40}H_{36.20}CdN_4O_{4.70}$	$C_{23}H_{20}CdN_2O_5$
Formula weight	681.26	516.81
Crystal system	Monoclinic	Triclinic
Space group	*C2/c*	*Pī*
a (Å)	11.553(2)	6.798(8)
b (Å)	14.353(1)	11.317(4)
c (Å)	19.165(1)	14.791(9)
α (°)	90	77.99(2)
β (°)	102.03(3)	70.81(2)
γ (°)	90	87.46(2)
V (Å^3)	3108.37(7)	1051.6(2)
Z	4	2
D_{calcd} (g/cm^3)	1.488	1.632
Absorption coefficient, mm^{-1}	0.749	1.076
F(000)	1401	520
Crystal size, mm	0.26 x 0.23 x 0.22	0.20 x 0.16 x 0.12
θ range, deg	2.294-26.372	2.969-28.388
Index range *h*, *k*, *l*	-14/14, -17/17, -23/20	-7/9, -15/15, -19/19
Reflections collected	18630	15054
Independent reflections (R_{int})	3150(0.0637)	5179 (0.0179)
Data/restraint/parameters	3150 / 26 / 238	5179 / 0 / 297
Goodness-of-fit on F^2	1.089	1.006
Final R_1, wR_2 ($I > 2\sigma(I)$)	0.0609, 0.1781	0.0209, 0.0583
Largest diff. peak and hole	1.064, -1.658	0.395, -0.490

Table S2 Selected Bond Lengths [Å] and Angles [º] for the **1** and **2**

Parameter	Value	Parameter	Value
1			
Cd1–O1	2.270(4)	Cd1–O1A	2.270(4)
Cd1–N1	2.273(3)	Cd1–N1A	2.273(3)
Cd1–O2	2.350(4)	Cd1–O2A	2.350(5)
O1A–Cd1–O1	169.00(2)	O1A–Cd1–N1	86.20(2)
O1–Cd1–N1	98.60(2)	O1A–Cd1–N1A	98.60(1)
O1-Cd1-N1A	86.20(2)	N1–Cd1–N1A	127.50(2)
O1A–Cd1–O2A	48.00(2)	O1–Cd1–O2A	122.50(2)
N1–Cd1–O2A	125.40(2)	N1A–Cd1–O2A	92.40(2)
N1–Cd1–O2	92.40(2)	N1A–Cd1–O2	125.40(2)
O2–Cd1–O2A	90.90(2)	O2A–Cd1–O2A	90.90(2)
O1A-Cd1-O2	48.00(2)		
2			
Cd1–N1	2.229(2)	Cd1–O1	2.234(1)
Cd1–O5	2.342(2)	Cd1–O4B	2.342(2)
Cd1–O1A	2.351(2)	Cd1–O3B	2.380(2)
O1−Cd1−O5	98.57(2)	N1−Cd1−O5	89.34(2)
N3−Cd1−N1A	91.55(2)	N1−Cd1−O4B	106.09(2)
O1−Cd1−O4B	141.37(2)	O5−Cd1−O4B	93.31(2)
N1−Cd1−O1A	101.01(2)	O1−Cd1−O1A	76.72(2)
O5−Cd1−O1A	169.59(2)	O4B−Cd1−O1A	86.95(2)
N1−Cd1−O3B	157.43(2)	O1−Cd1−O3B	89.82(2)
O5−Cd1−O3A	79.22(2)	O4B−Cd1−O3B	55.38(2)
O1A−Cd1−O3B	91.39(2)		

Symmetry codes for **1**: A = A: 1-*x*, *y*, 0.5-*z*; for **2**: A:1-*x*,1-*y*,1-*z*; B: -*x*,1-*y*,1-*z*.

Table S3. Simulated in different environments at room temperature

serial number	Inclusion factor
S-1	Fe^{3+}+ distilled water
S-2	Fe^{3+}+ tap water
S-3	Fe^{3+}+ Cd^{2+}, Ag^{+}, Cu^{2+}, Pb^{2+}
S-4	Fe^{3+}+ Zn^{2+}, Ni^{2+}, Co^{2+}, Sm^{3+}
S-5	Fe^{3+}+ Gd^{3+}, Al^{3+}, Hg^{2+}, La^{3+}
S-6	Fe^{3+}+ tap water + all cation
S-7	acac + distilled water
S-8	acac + tap water
S-9	acac + EtOH, MeCN, DMF
S-10	acac + DMSO, DCM, EG
S-11	acac + MeOH, AT, NMP
S-12	acac + tap water +all organic solvents

S stands for simulation, Ethanol (EtOH), Acetonitrile (MeCN), *N,N*-dimethylformamide (DMF), Dimethyl sulfoxide (DMSO), dichloromethane (DCM), methanol (MeOH), Acetone(AT), Acetylacetone (acac), Ethylene glycol (EG) and N-Methyl pyrrolidone (NMP).

Table S4. Comparison of the sensitivities of **1** and **2** for acac with related CPs

CPs	LOD/M	Ref
$\{[(CH_3)_2NH_2][Zn(FDA)(BTZ)_2]\}_n$	6.47×10^{-7}	[14]
$\{[Zn_2(XN)_2(IPA)_2]\cdot2H_2O\}_n$	0.25×10^{-7}	[17]
$\{[Zn_3(bbib)_2(ndc)_3]\cdot2DMF\cdot2H_2O\}_n$	0.10×10^{-7}	[16]
$\{[Zn(XL)_2](ClO_4)_2\cdot6H_2O\}_n$	1.72×10^{-7}	[15]
1	2.45×10^{-6}	This work
2	1.40×10^{-6}	This work

H_2FDA = furan-2,5-dicarboxylic acid, HBTZ = 1*H*-benzotriazole, XN = 4'-(4-pyridine)4,2':2',4''-terpyridine, IPA = isophthalic acid, bbib = 1,3-bis(benzimidazolyl)benzene, H_2ndc = 1,4-naphthalenedicarboxylic acid, XL=*N*,*N*'-bicyclo[2.2.2]oct-7-ene-2,3,5,6-tetracarboxdiimide bi(1,2,4-triazole).

Table S5. Comparison of the sensitivities of **1** and **2** with previously reported CPs to Fe^{3+} ions

CPs	LOD/M	Ref
Cd-DTA	0.82×10^{-6}	[11]
Zn-DTA	1.03×10^{-6}	[11]
$[Cd(PAM)(4\text{-bpdb})_{1.5}]DMF$	0.3×10^{-6}	[18]
1	8.51×10^{-6}	This work
2	0.10×10^{-6}	This work

H_2DTA = 2,5-di(1H-imidazol-1-yl)terephthalic acid, PAM= 4,4-methylenebis(3-hydroxy-2-naphthalene-carboxylic acid), 4-bpdb = 1,4-bis(4-pyridyl)-2,3-diaza-1,3-butadiene

Fig. S1. 1D chain of metal Cd(II) growth by 1,4-PDA^{2-} and L ligands.

Fig. S2. One 1D double straight-line of metal Cd(II) growth by 1,8-NDC^{2-} ligands and one unit [Cd(L)] of metal Cd(II) growth by L ligands.

Fig. S3. The infrared spectrum of **1** and **2.**

Fig. S4. The PXRD pattern of the bulk sample is consistent with the simulated pattern of the single crystal structure in **1** and **2.**

Fig. S5. PXRD patterns of **1** and **2** for various organic small molecules.

Fig. S6. PXRD patterns of **1** and **2** for various anions in cation solution.

Fig. S7. (a)The PXRD patterns of **1** in different pH solutions; (b) The PXRD patterns of **2** in different pH solutions.

Fig. S8. The change of the fluorescence emission intensity of **1** and **2** in different pH solutions.

Fig. S9. TGA curves of **1** and **2**

Fig. S10. Quantum yield measurement for **1** (a)and **2** (b).

Fig. S11. Soild luminescence lifetime of **1** (a) and **2** (b).

Fig. S12. Time-dependent emission spectra of **1** and **2** suspended in aqueous solutions.

Fig. S13. Comparison of the luminescence intensity of **1** (a) and **2** (b) in the presence of mixed organic solvents.

Fig. S14. Histogram of **1** (a) and **2** (b) dispersed in aqueous solution in the presence of different metal cation. Solvent: DMSO/H_2O (1:1, v/v).

Fig. S15. Fluorescence emission spectra of Fe^{3+} ions and other metal ions in **1** (a) and **2** (b) at room temperature.

Fig. S16. (a) PXRD patterns of **1** or **2** dispersed in water, **1** or **2** dispersed in a Fe^{3+} solution and the recycled sample; (b) PXRD patterns of **1** or **2** dispersed in water, **1** or **2** dispersed in an acac solution and the recycled sample. Solvent: DMSO/H_2O (1:1, v/v).

Fig. S17. (a) **1** and **2** are the first time in water, the first cycle, the first time to add Fe^{3+}, the second cycle and the fifth cycle of fluorescence emission intensity. (b) **1** and **2** are the first time in water, the first cycle, the first time to add acac, the second cycle and the fifth cycle of fluorescence emission intensity. Solvent: DMSO/H_2O (1:1, v/v).

Fig. S18. (a) Effects of pH on the fluorescence maxima of **1** + acac (circle) and **1** + Fe^{3+} (triangle); (a) Effects of pH on the fluorescence maxima of **2** + acac (circle) and **2** + Fe^{3+} (triangle). Solvent: DMSO/H_2O (1:1, v/v)

Fig. S19. The relationship between the fluorescence intensity of Fe^{3+} (a) or acac (b) detected over time in different simulated environments in **1**.

Fig. S20. The relationship between the fluorescence intensity of Fe^{3+} (a) or acac (b) detected over time in different simulated environments in **2**.

Fig. S21. Spectral overlap between the absorption spectra of Fe^{3+} ions and the excitation spectra of **1** and **2**.

Fig. S22. Spectral overlap between the absorption spectra of acac ions and the excitation spectra of **1** and **2**.

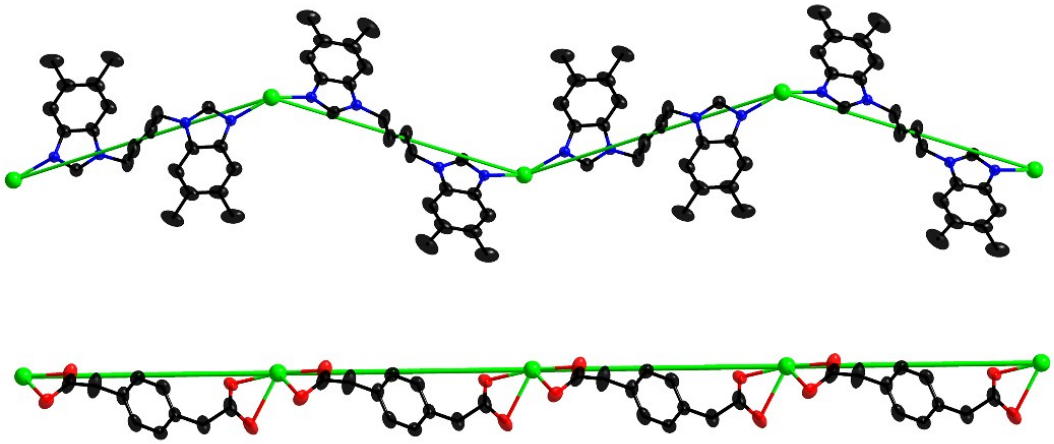

Fig. S1. 1D chain of metal Cd(II) growth by 1,4-PDA^{2-} and L ligands.

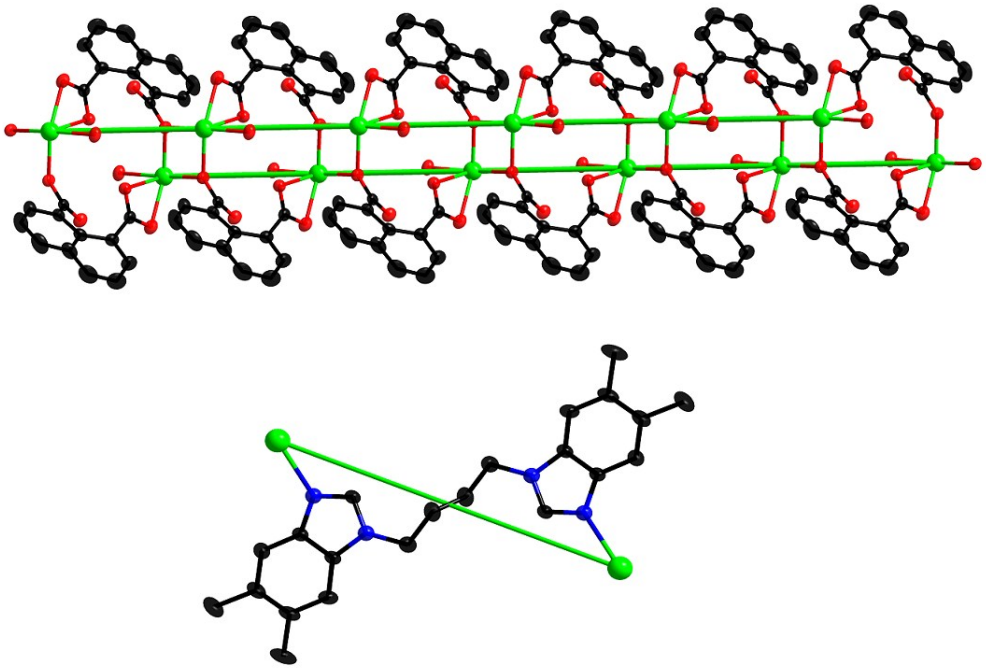

Fig. S2. One 1D double straight-line of metal Cd(II) growth by 1,8-NDC^{2-} ligands and one unit [Cd(L)] of metal Cd(II) growth by L ligands.

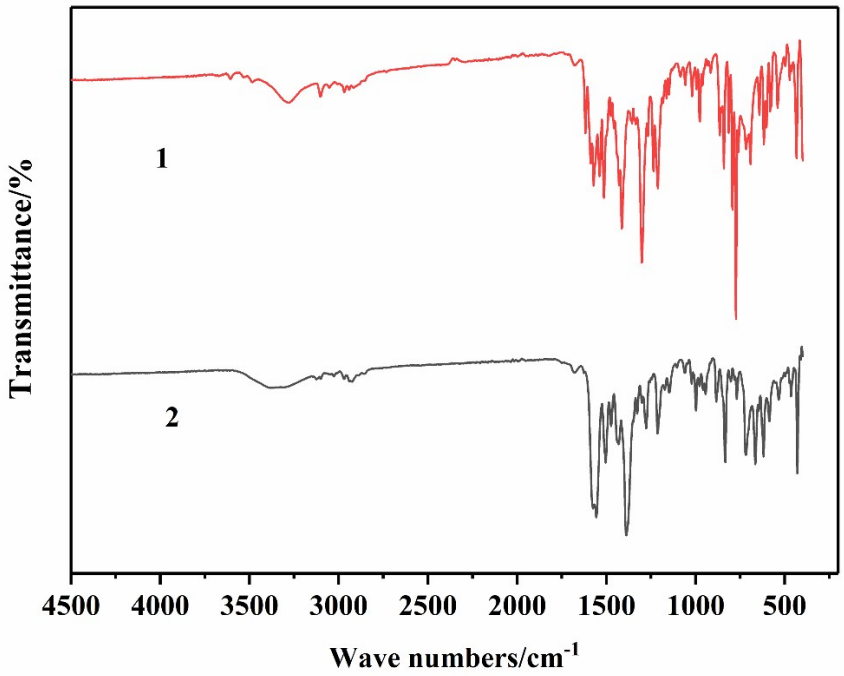

Fig. S3. The infrared spectrum of **1** and **2.**

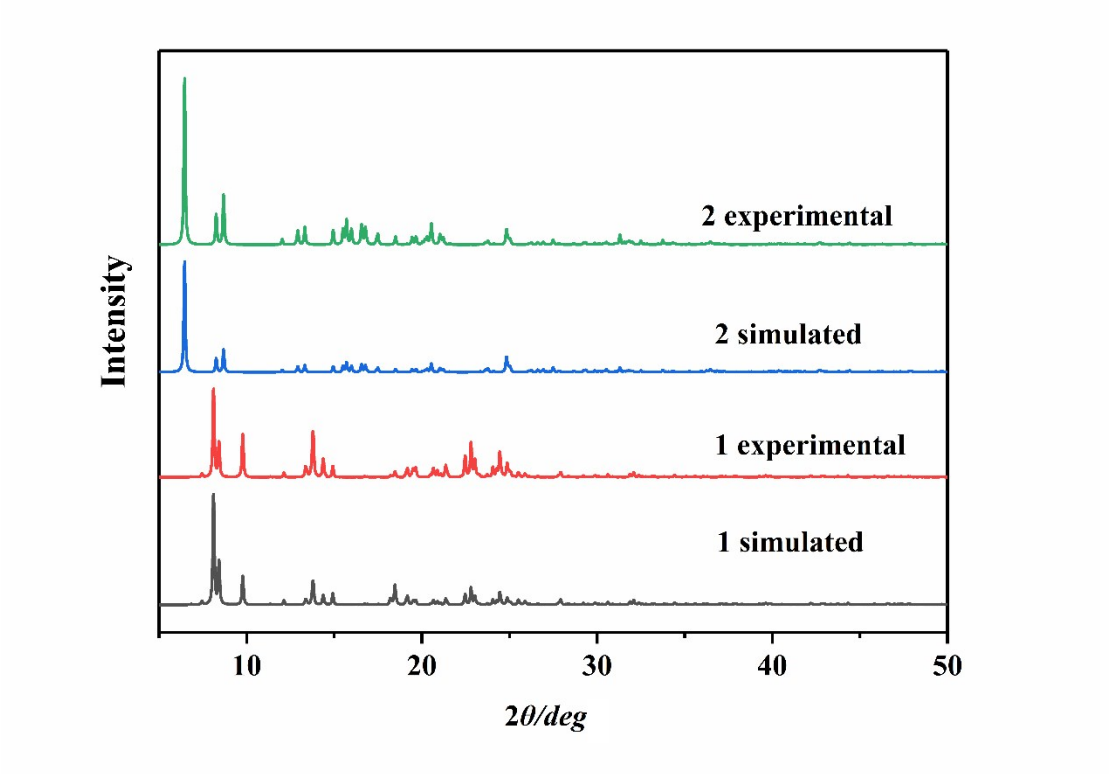

Fig. S4. The PXRD pattern of the bulk sample is consistent with the simulated pattern of the single crystal structure in **1** and **2.**

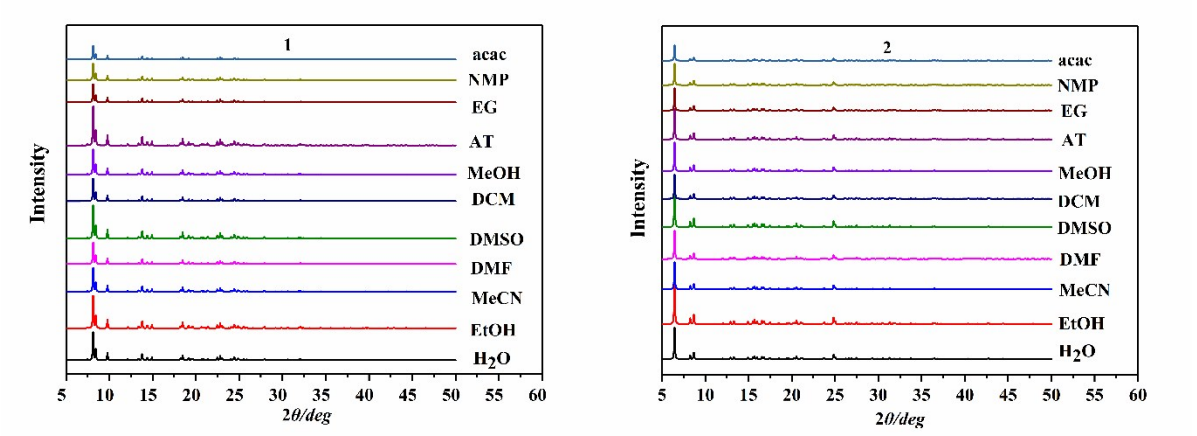

Fig. S5. PXRD patterns of **1** and **2** for various organic small molecules.

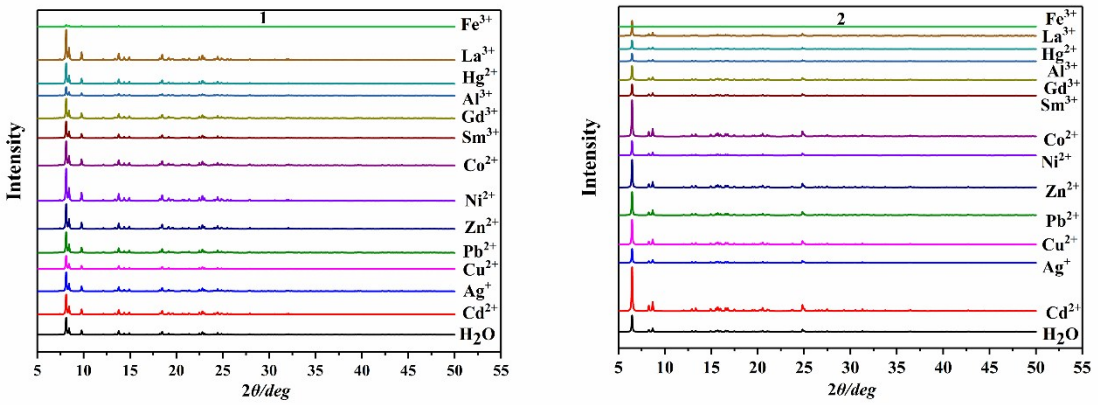

Fig. S6. PXRD patterns of **1** and **2** for various anions in cation solution.

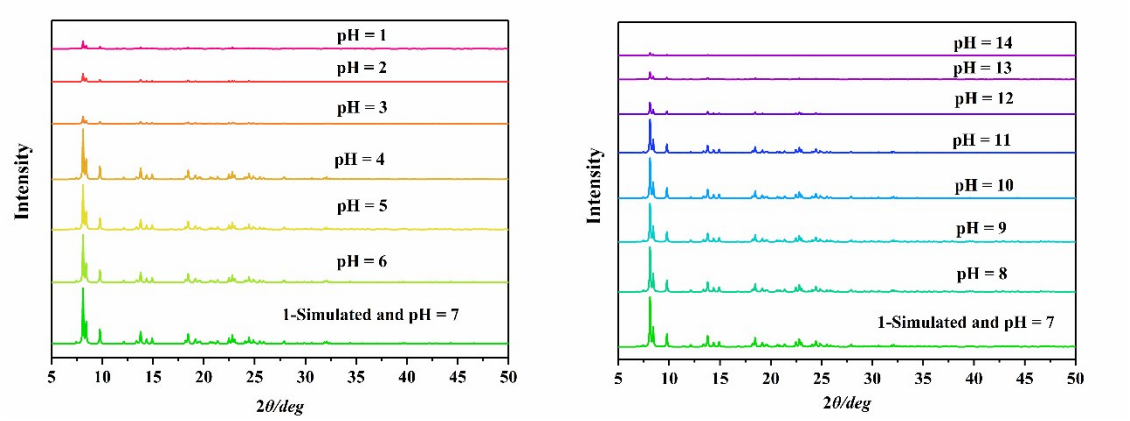

(a)

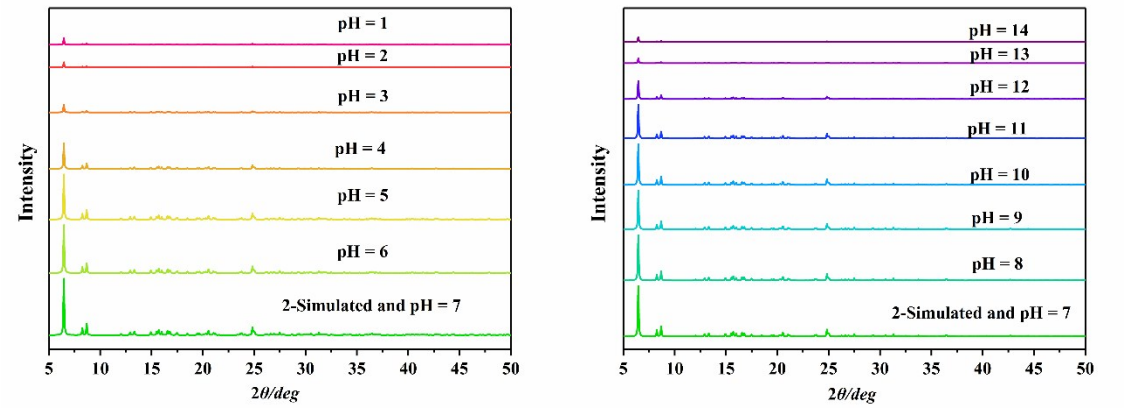

(b)

Fig. S7. (a)The PXRD patterns of **1** in different pH solutions; (b) The PXRD patterns of **2** in different pH solutions.

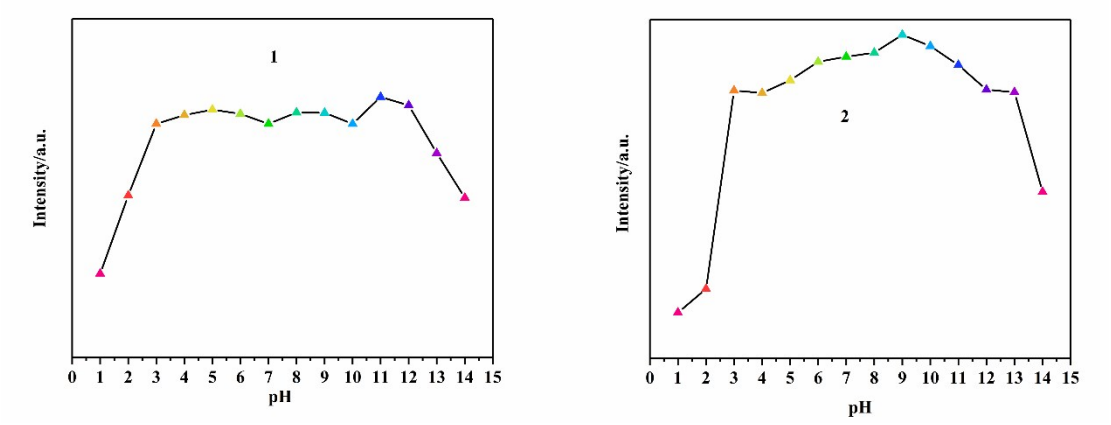

Fig. S8. The change of the fluorescence emission intensity of **1** and **2** in different pH solutions.

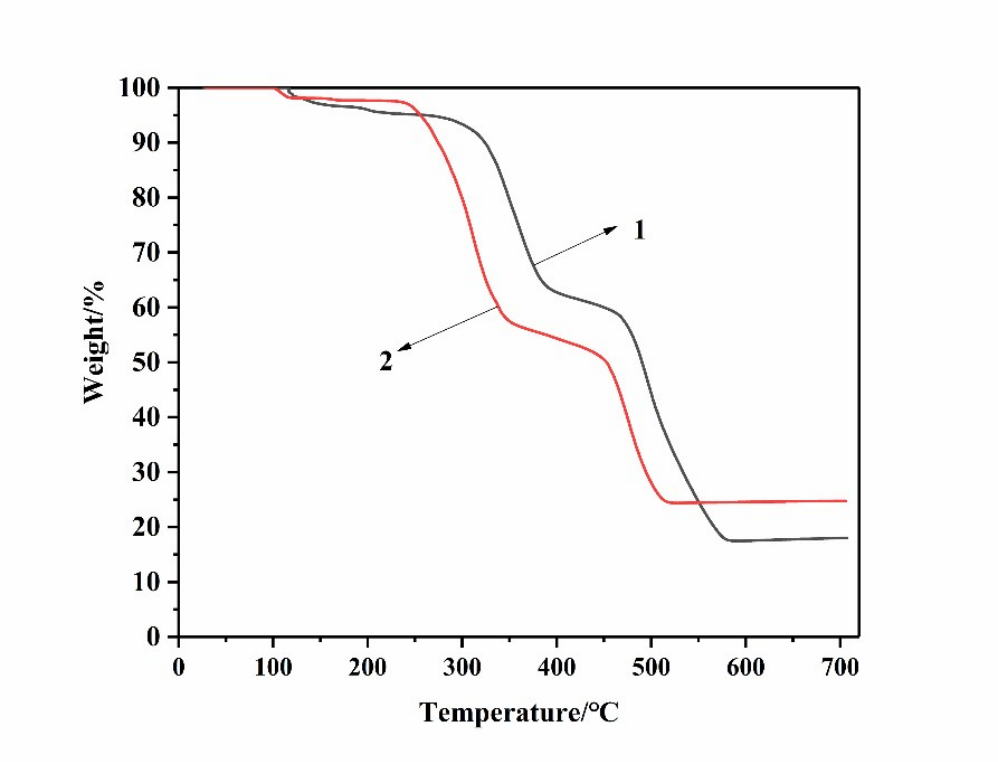

Fig. S9. TGA curves of **1** and **2**

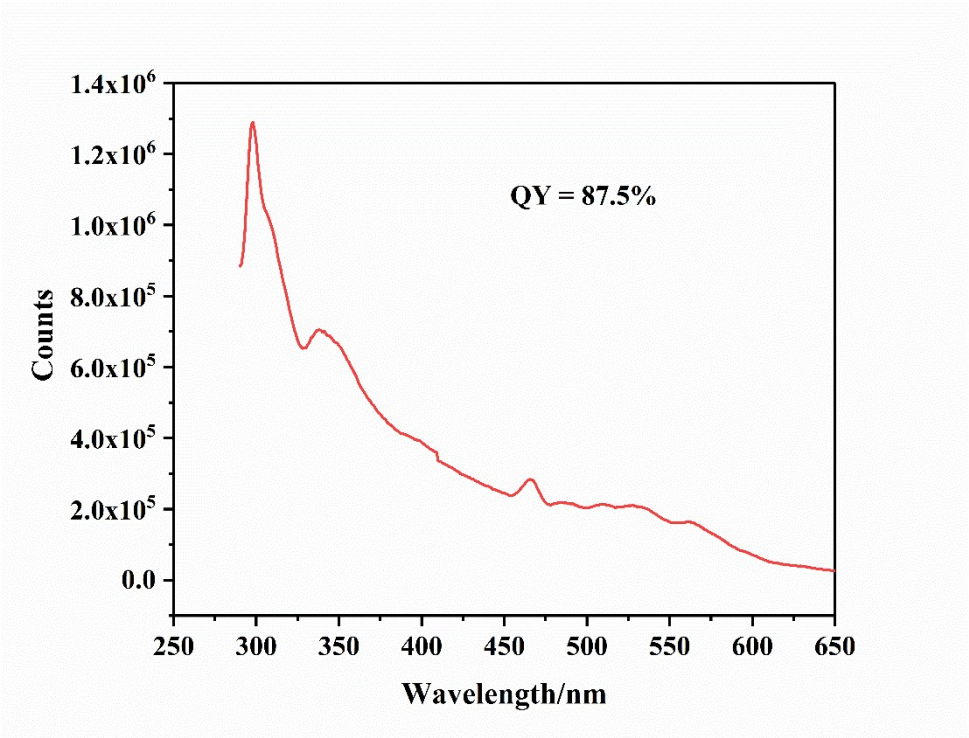

(a)

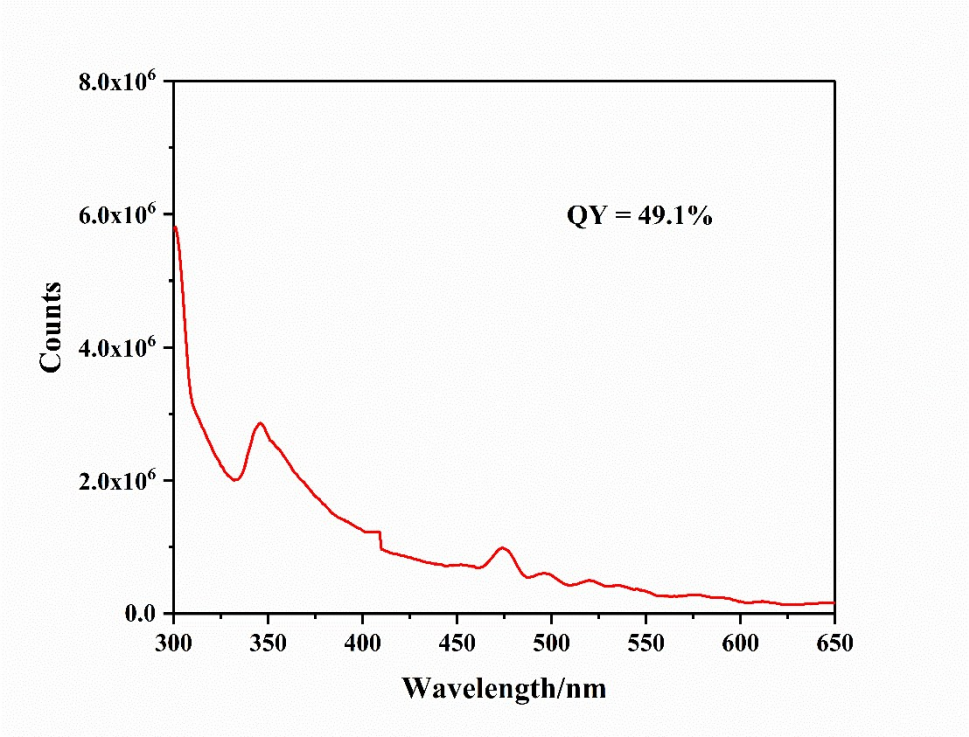

(b)

Fig. S10. Quantum yield measurement for **1** (a) and **2** (b).

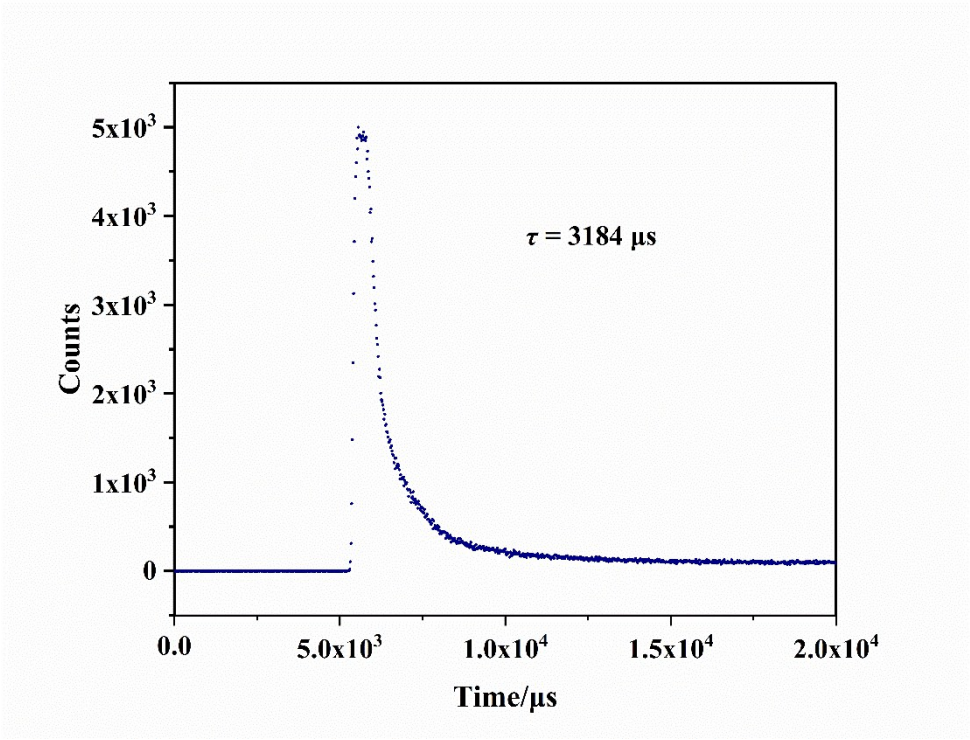

(a)

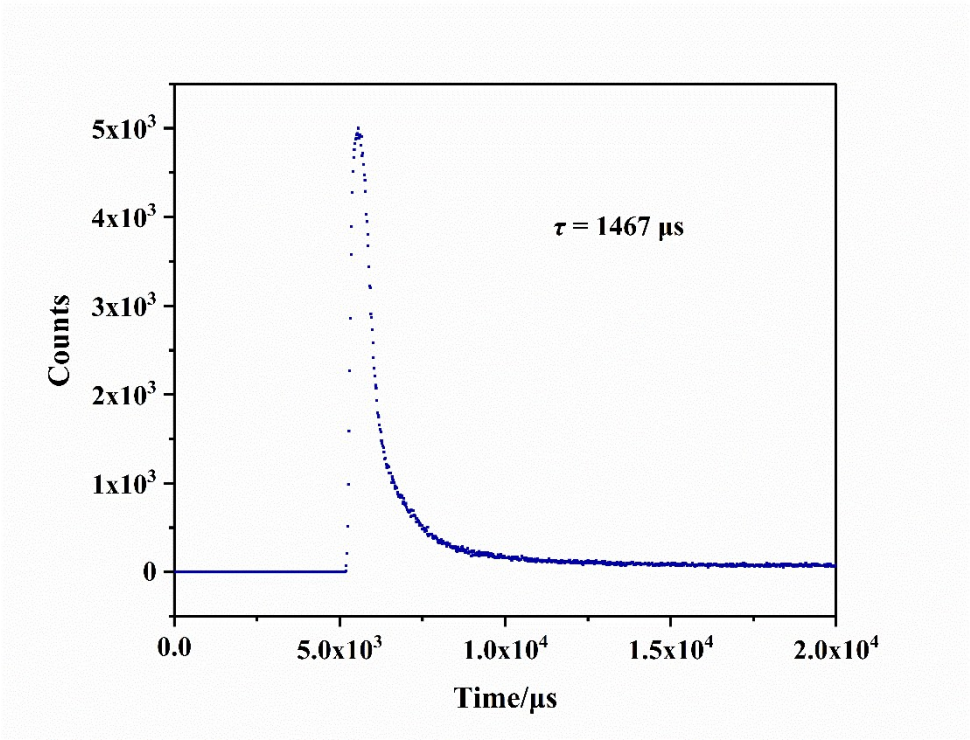

(b)

Fig. S11. Soild luminescence lifetime of **1** (a) and **2** (b).

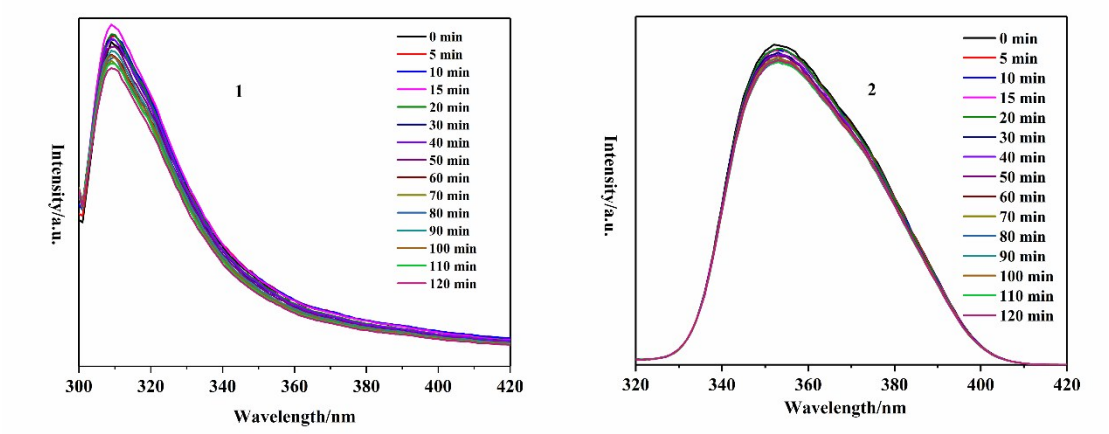

Fig. S12. Time-dependent emission spectra of **1** and **2** suspended in aqueous solutions.

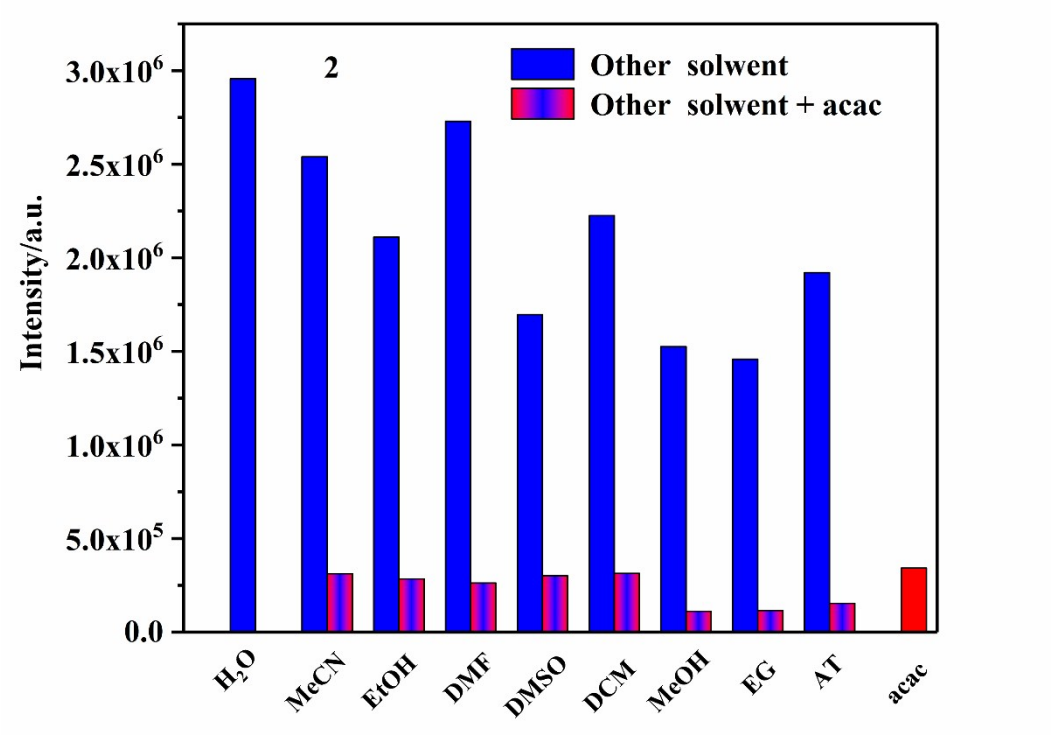

(a)

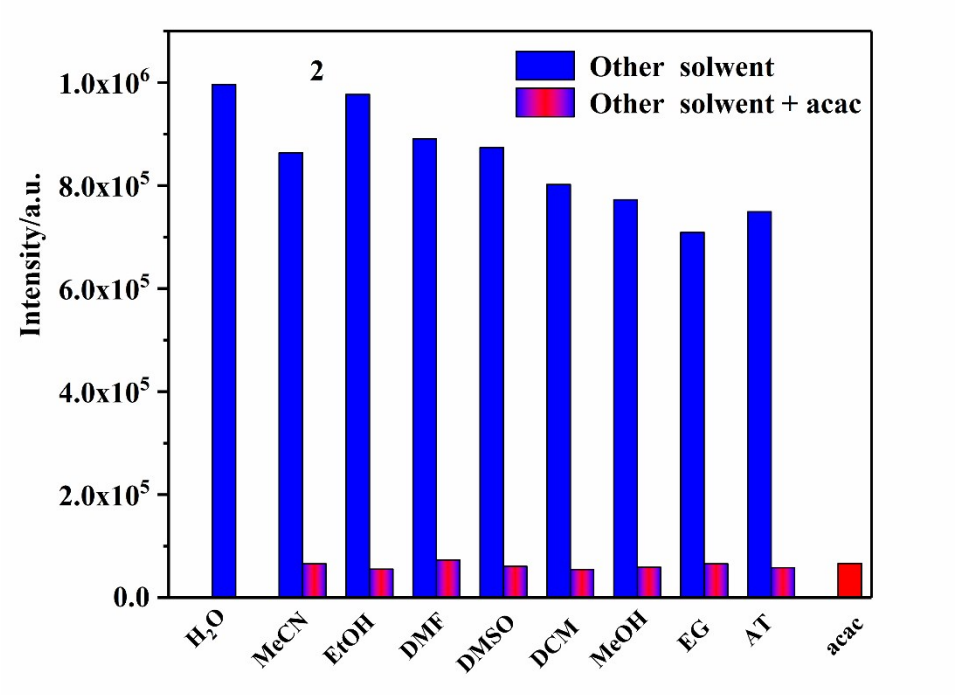

(b)

Fig. S13. Comparison of the luminescence intensity of **1** (a) and **2** (b) in the presence of mixed organic solvents.

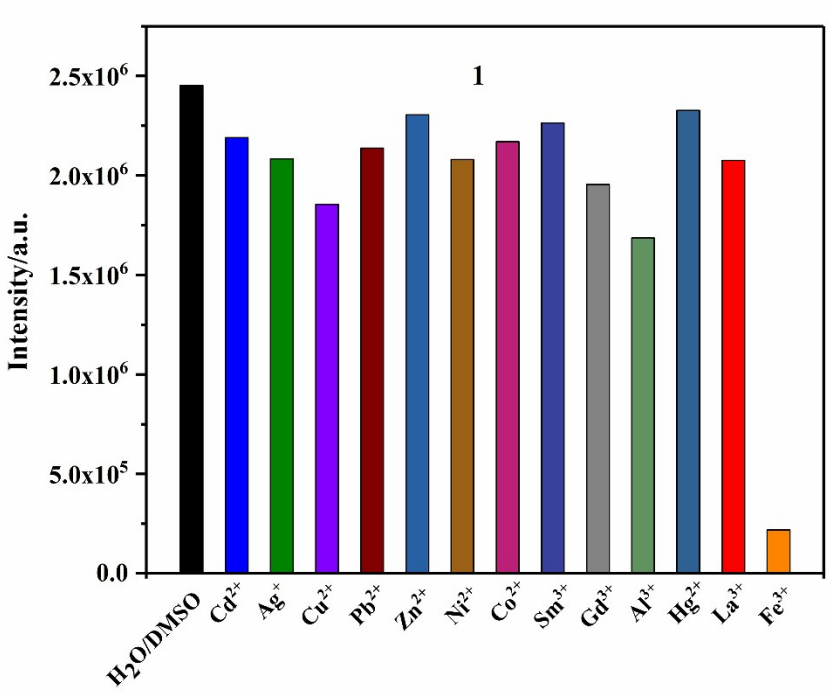

(a)

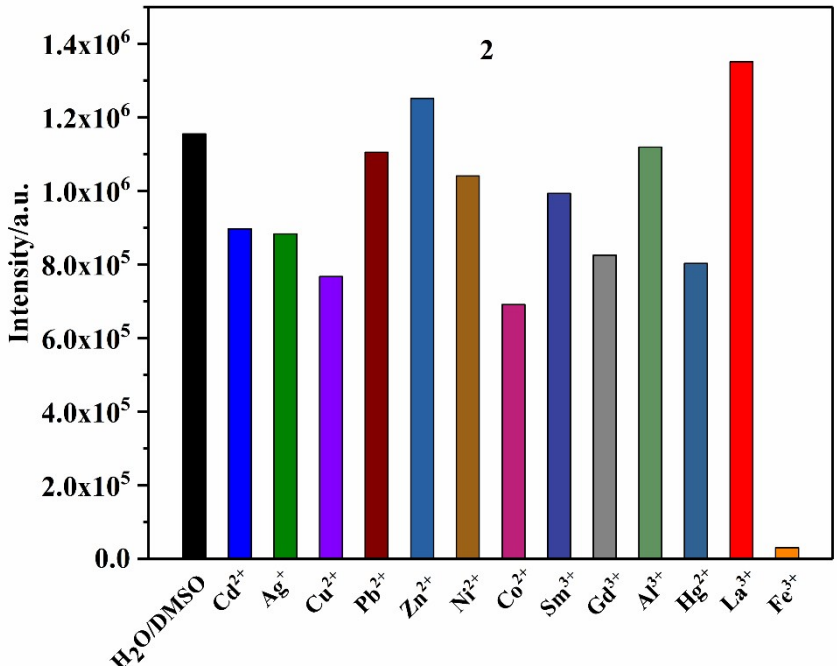

(b)

Fig. S14. Histogram of **1** (a) and **2** (b) dispersed in aqueous solution in the presence of different metal cation. Solvent: DMSO/H_2O (1:1, v/v).

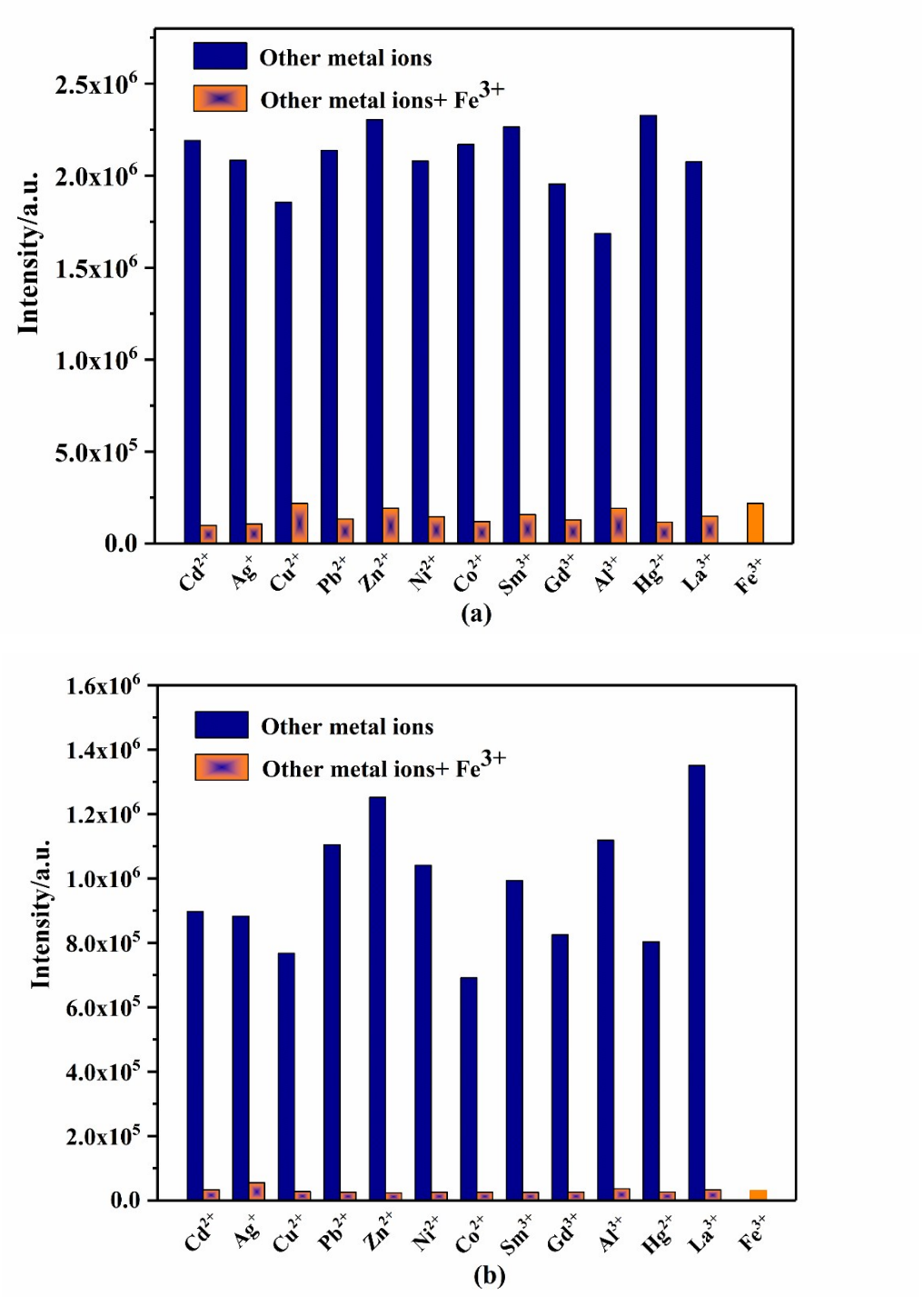

Fig. S15. Fluorescence emission spectra of Fe^{3+} ions and other metal ions in **1** (a) and **2** (b) at room temperature.

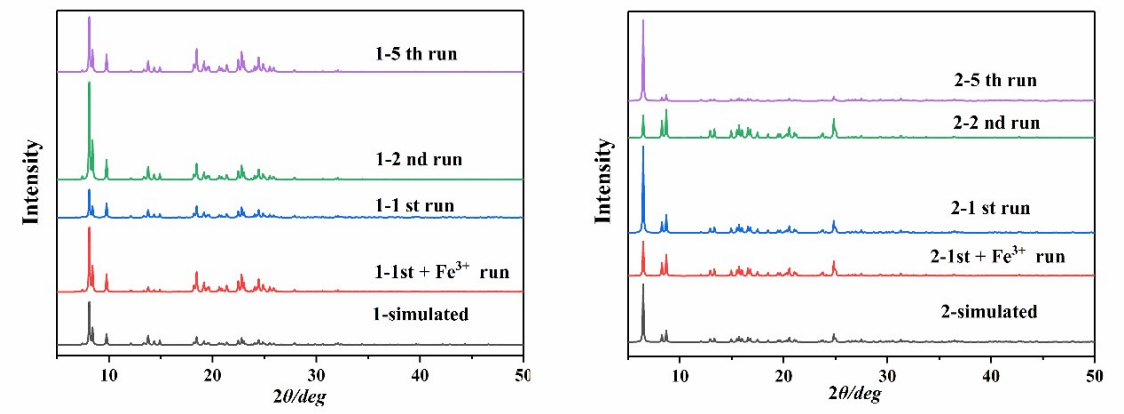

(a)

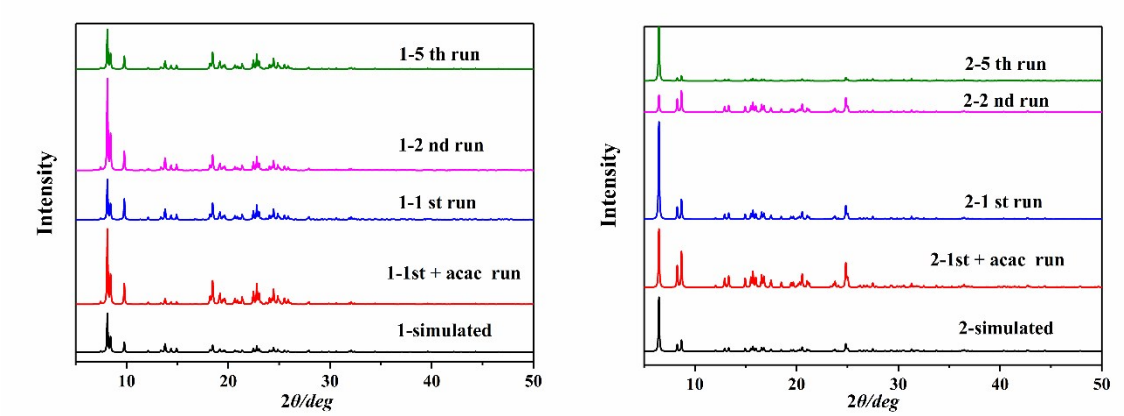

(b)

Fig. S16. (a) PXRD patterns of **1** or **2** dispersed in water, **1** or **2** dispersed in a Fe^{3+} solution and the recycled sample; (b) PXRD patterns of **1** or **2** dispersed in water, **1** or **2** dispersed in an acac solution and the recycled sample. Solvent: DMSO/H_2O (1:1, v/v).

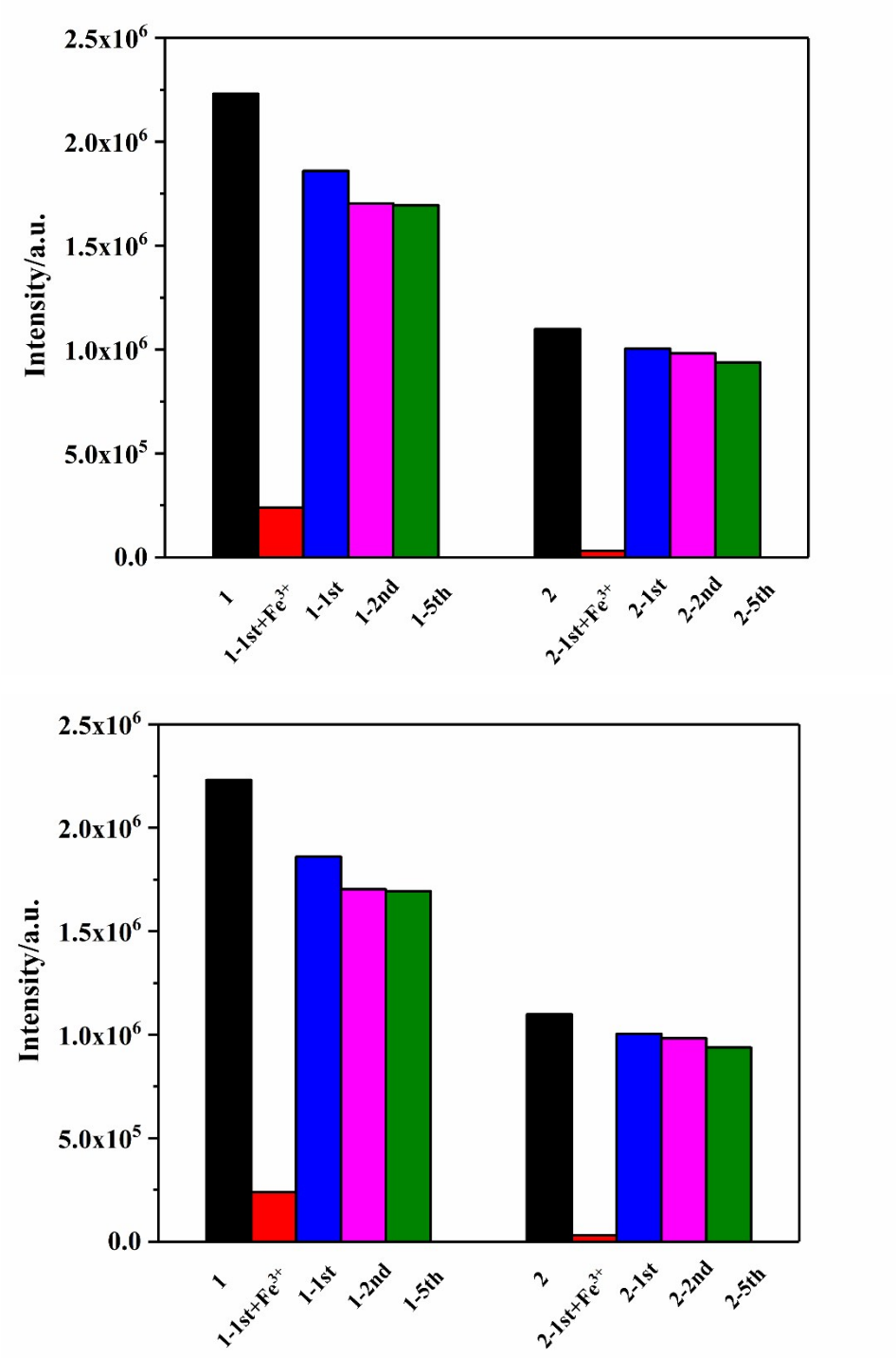

Fig. S17. (a) **1** and **2** are the first time in water, the first cycle, the first time to add Fe^{3+}, the second cycle and the fifth cycle of fluorescence emission intensity. (b) **1** and **2** are the first time in water, the first cycle, the first time to add acac, the second cycle and the fifth cycle of fluorescence emission intensity. Solvent: DMSO/H_2O (1:1, v/v).

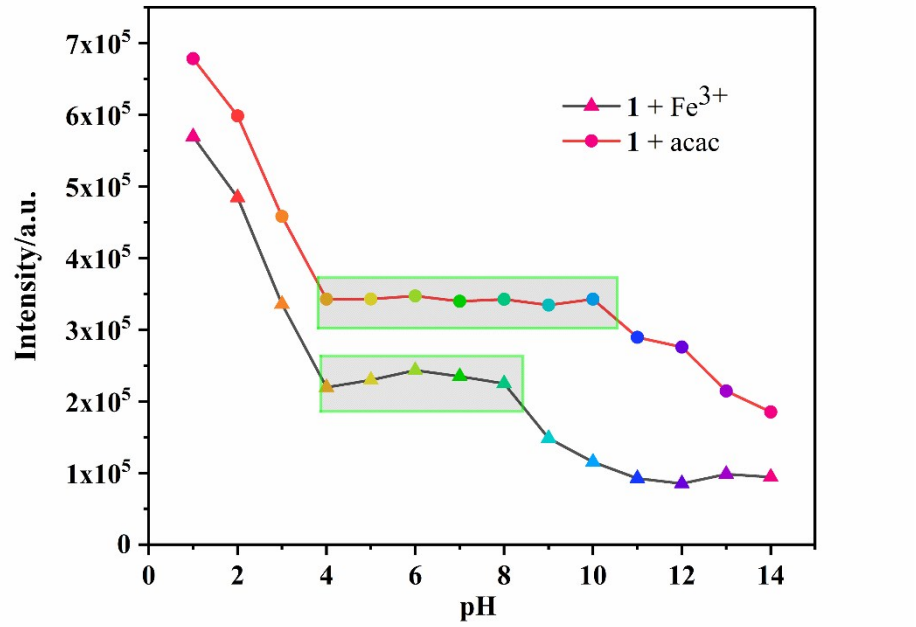

(a)

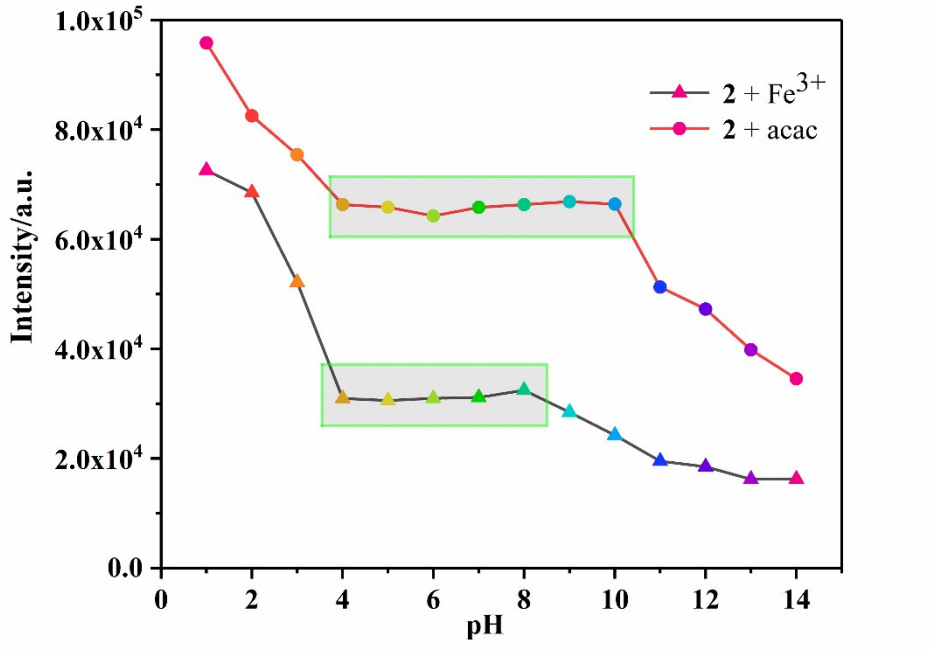

(b)

Fig. S18. (a) Effects of pH on the fluorescence maxima of **1** + acac (circle) and **1** + Fe^{3+} (triangle); (a) Effects of pH on the fluorescence maxima of **2** + acac (circle) and **2** + Fe^{3+} (triangle). Solvent: DMSO/H_2O (1:1, v/v).

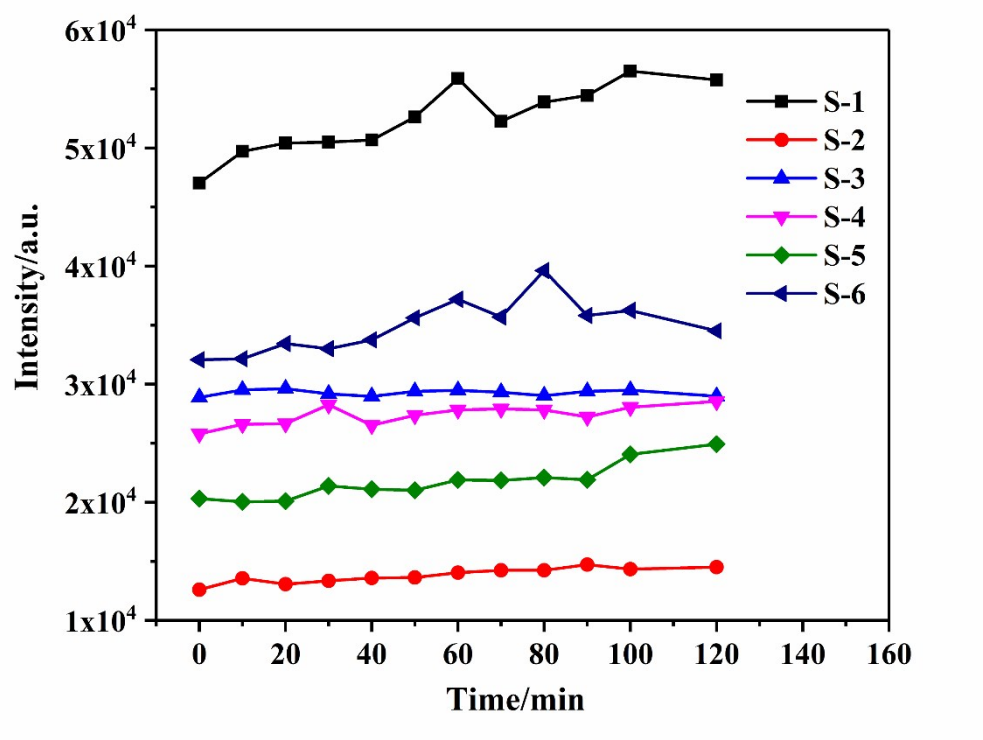

(a)

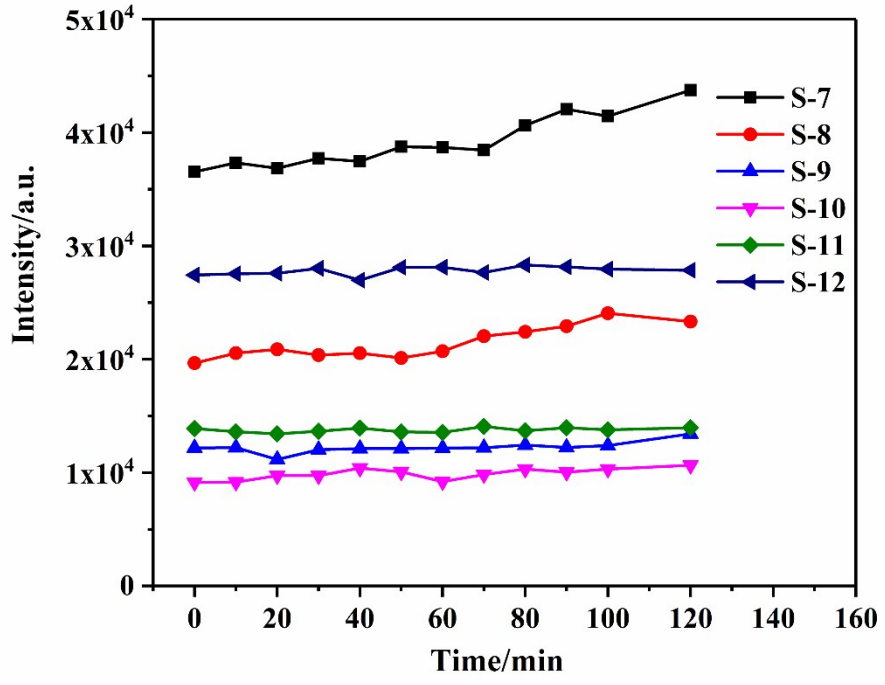

(b)

Fig. S19. The relationship between the fluorescence intensity of Fe^{3+} (a) or acac (b) detected over time in different simulated environments in **1**.

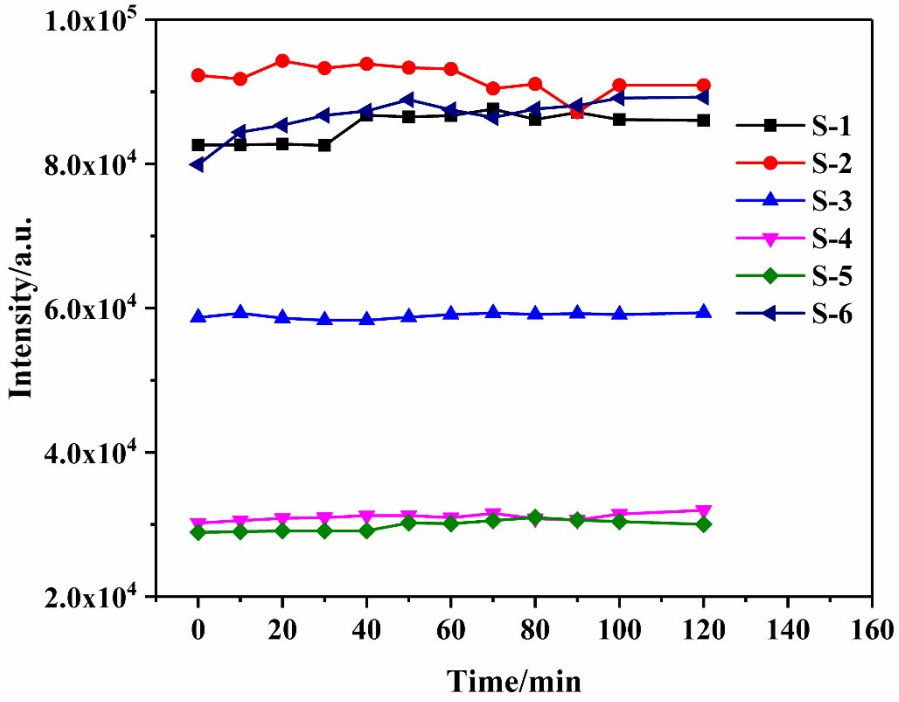

(a)

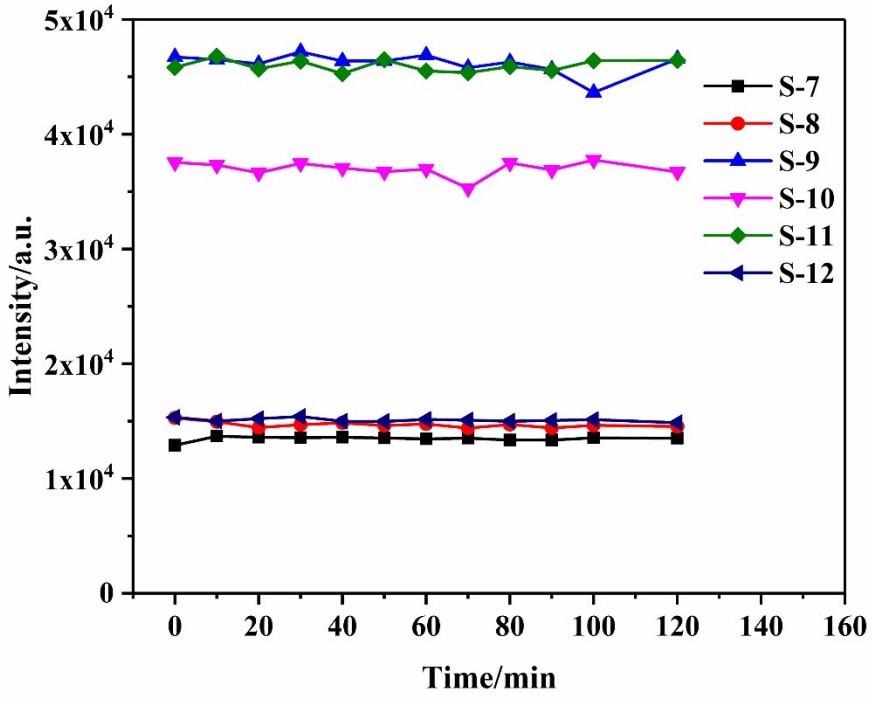

(b)

Fig. S20. The relationship between the fluorescence intensity of Fe^{3+} (a) or acac (b) detected over time in different simulated environments in **2**.

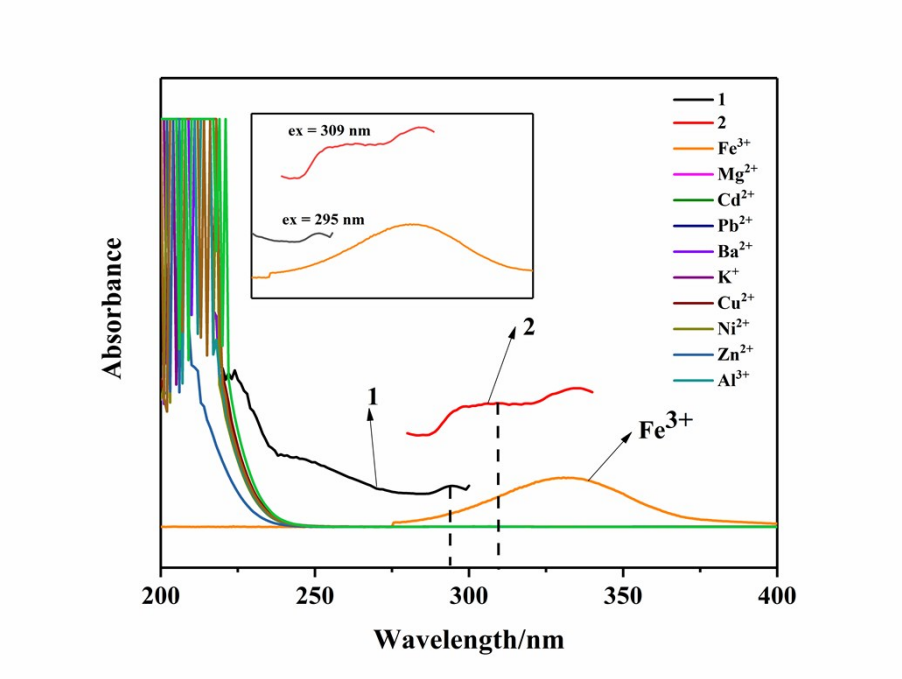

Fig. S21. Spectral overlap between the absorption spectra of Fe^{3+} ions and the excitation spectra of **1** and **2**.

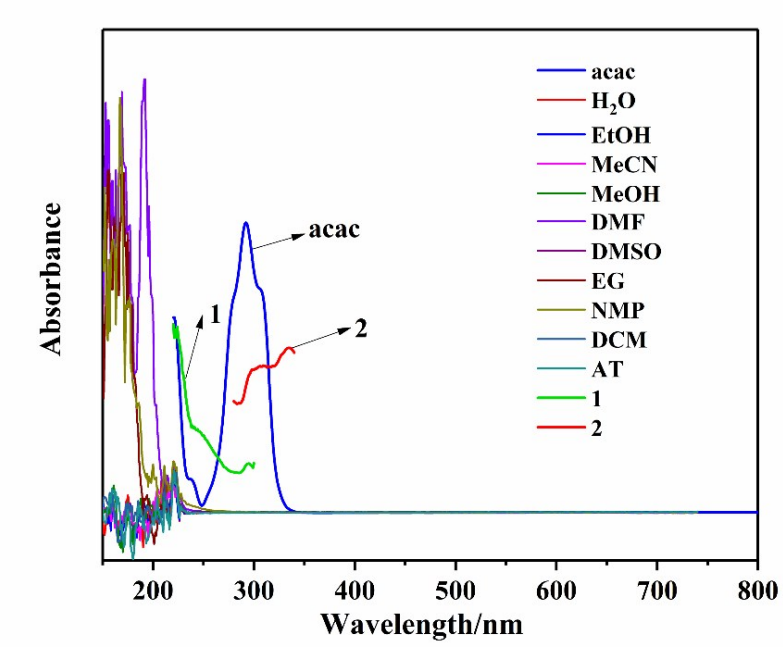

Fig. S22. Spectral overlap between the absorption spectra of acac ions and the excitation spectra of **1** and **2**.